In: Cataracts: Causes, Symptoms, and Surgery
Editor: Camila M. Hernandez, pp. 109-124

ISBN: 978-1-61668-955-1

Chapter 4

INTRAOCULAR LENS SURFACE PROPERTIES INVESTIGATED WITH NANOMETER SCALE RESOLUTION USING ATOMIC FORCE MICROSCOPY

Marco Lombardo[1,2*], Giuseppe Lombardo[3], Giovanni Carbone[3,4], Maria P. De Santo[3], Sebastiano Serrao[5] and Riccardo Barberi[3]

[1] Vision Engineering, Rome, Italy
[2] IRCCS G.B. Bietti Foundation, Rome, Italy
[3]CNR IPCF Unit of Support of Cosenza, c/o Department of Physics, University of Calabria, Rende (CS), Italy
[4] Department of Engineering Science, University of Oxford, Oxford, UK
[5] SerraoLaser, Rome, Italy

ABSTRACT

The posterior capsular opacification (PCO) represents the most significant cause of visual impairment after cataract surgery. During the last decade, a great deal of work has been conducted to analyze which intraocular lens (IOL) property could primarily influence the rate and severity of PCO. It was found that the geometrical design of IOL affects the rate of PCO and it has been proven that a sharp IOL posterior optic edge improves the prevention of PCO. On the other hand, the surface properties of the IOL biomaterial also appeared to play a relevant role in preventing PCO.

In this work we investigate, with nanometer scale resolution, the physical properties of the surface for the IOL biomaterials currently in use in the clinical environment: poly-methyl-methacrylate (PMMA), silicone, hydrophilic acrylic and hydrophobic acrylic. An Atomic Force Microscope was used both to measure the topography and adhesiveness of IOLs' optic surface. Analysis of IOLs was performed in liquid environment.

* Corresponding author: e-mail: mlombardo@visioeng.it, Via Adda 7 – 00198 Rome (ITALY).

The topography measurements of the IOLs' optic were performed using an Autoprobe CP (Veeco, Sunnyvale, CA) operated in the contact mode and V-shaped cantilevers with a 0.01 Newton/meter (N/m) nominal elastic constant. The topography of IOLs' surface revealed different features strongly correlated with both the lens biomaterial and the processes used to manufacture the IOLs. The root mean square (*RMS*) roughness of the IOL optic surface was significantly different between lenses of various materials ($P<0.001$): hydrophobic acrylic and silicone IOLs have shown the lowest surface roughness, i.e., 3.8 ± 0.2 nanometer (nm) and 4.0 ± 0.5 nm respectively, whereas the highest surface roughness (7.0 ± 0.6 nm) was measured for PMMA lenses. The mean *RMS* roughness of the hydrophilic acrylic lens was 5.0 ± 0.5 nm.

The adhesive properties of IOLs' surface was studied using a NanoScope III (Veeco, Sunnyvale, CA), operated in the Force-vs-Distance (*f-d*) mode with rectangular cantilevers of nominal elastic constant of 10 N/m. A statistically significant correlation between adhesion properties of each IOL and their constituent material was measured ($P<0.001$). The hydrophobic acrylic IOL exhibited the largest mean value for the adhesive force (283.75 ± 0.14 nanoNewton, nN) followed by the hydrophilic acrylic (84.76 ± 0.94 nN), PMMA (45.77 ± 0.47 nN) and silicone IOLs (2.10 ± 0.01 nN).

AFM was demonstrated to be an effective and accurate tool for the analysis of the IOL's optic. The surface properties of the biomaterials used to manufacture IOLs are important factors as they can influence the incidence and severity of PCO. While further studies are necessary to elucidate the mechanism of PCO development and the interface interactions between the IOL and capsule, the results from this work may enhance the theory of manufacturing materials with smooth and adhesive optic surface to prevent PCO.

INTRODUCTION

Over the past decade, cataract patients have benefited from dramatic improvements in phacoemulsification systems and fluidics as well as new intraocular lens (IOL) design and materials. Nevertheless, the posterior capsular opacification (PCO) still represents a significant cause of visual impairment after cataract surgery, with a mean incidence of approximately 5-7% at a mean of three years after surgery [1,2,3,4]. The main surgical strategies to minimize the risk of PCO are considered to perform a central, well-positioned curvilinear capsulorhexis overlapping the anterior edge of the IOL optic as well as to remove as many of the equatorial lens epithelial cells (LECs) as possible through rigorous cortical clean-up[5,6]. On the other hand, the prevention of PCO is mainly attributed to the development of new IOL materials and optic designs [7].

PCO is considered to have a multifactorial pathogenesis and LECs are considered to be the main cellular precursors of this process [8]. LECs lie immediately adjacent to the inner surface of the lens capsule and remain attached to the capsular bag after cataract extraction. These cells can differentiate, proliferate and migrate onto the IOL surface and onto the lens capsule leading to capsule opacification [9]. The observation of leukocytes, macrophages and giant cells that adhere to the IOL surface suggests that the IOL implantation, besides the inflammatory reaction induced by the surgery, gives rise to a foreign-body reaction [10,11]. Thereafter, inflammatory cells may contribute to the development of PCO by activating LEC migration and promoting their differentiation and proliferation [12].

A great deal of work has been carrying out to study how the biomaterial and the surface properties of the IOL can influence the inflammatory reaction following IOL implantation as well as the adhesion and migration of LECs onto the IOL optic [11,13,14]. A sharp posterior optic edge design of the IOL has been associated with a substantial decrease in PCO incidence [3,7,15,16,17]. It is thought that, by pressing against the posterior capsule, the square-edge component mechanically prevents cell migration in the space between the IOL and the capsular bag. The capsular bend created at the posterior optic edge provides a perpendicular discontinuity that has been shown to effectively block LEC migration in experimental studies [18]. It is not completely clear, however, how a sharp optic edge alone can provide a substantial barrier when a bend or a firm contact of the IOL to the capsule are not formed [15,19]. Numerous researchers pointed out the importance of the type of IOL material, after demonstrating that acrylic and second generation silicone IOLs were associated with less PCO compared to polymethylmethacrylate (PMMA) IOL [20,21,22,23]. The different physical properties of the surface optic of the IOL biomaterial, like the adhesiveness of the material to the capsule and the surface roughness, are factors considered to be responsible for this clinical observation [24,25]. On the other hand, the mechanism by which the IOL biomaterial may influence LEC behavior still remains controversial [26].

Since the chemico-physical properties of the IOL optic surface represent the main factors that can influence the interfacial interactions between the IOL and the lens capsule environment, LEC behaviour may be greatly influenced by the surface properties of the IOL implanted, either its morphology or adhesiveness. In this study, we analyzed the surface properties of four different IOL materials currently used in ophthalmic surgery by exploiting the Atomic Force Microscopy (AFM) technique.

MATERIALS AND METHODS

Four types of posterior chamber IOLs were examined in this study: single piece PMMA, second generation three-piece silicone, single piece hydrophilic acrylic and three-piece hydrophobic acrylic. IOL specifications are summarized in table 1. The range of refractive power was between 17 and 25 diopters (D) for all the IOLs tested. Two samples for each IOL biomaterial were used either for topography or adhesion measurements.

The rigid PMMA lens (model 512B, Soleko, Italy) was fabricated from PERSPEX CQ poly(methylmethacrylate) and manufactured by a computerized lathe cutting. The hydrophobic acrylic lens (model MA60AC, Alcon, USA) is an aromatic acrylate-methacrylate copolymer. The primary monomers used in the synthesis of the AcrySof IOL material are 2-phenylethylacrylate (PEA) and 2-phenylethylmethacrylate (PEM). The hydrophilic acrylic (hydrogel) lens (model Akreos Fit, Bausch & Lomb, USA) is a polyhydroxyethylmethacrylate (HEMA) copolymer. The silicone IOL (model 911A, Pharmacia & Upjohn, Sweden) is a dimethyl siloxane-diphenyl siloxane copolymer silicone elastomer. Either the acrylic or silicone lenses are manufactured by a cast-molding process; they are flexible and foldable materials.

Before performing the measurement, each IOL was removed from its sterile pack with an atraumatic forceps and placed on specially designed Teflon environmental cell (figure 1). The sample was hold with the anterior surface optic side facing downward by a steel spring.

Accordingly, the analysis was performed on the posterior surface of each lens, i.e., the surface relevant for the IOL-cell-capsule interactions.

Table 1. Intraocular lens optic specifications

IOL Material	IOL Type
PMMA	Model 512B, 5-mm biconvex, rigid, unfoldable disk optic (Soleko SpA, Pontecorvo, Italy)
Hydrophobic Acrylic	Model MA60AC 6.00 mm biconvex soft, foldable, disk UV absorbing optic posterior chamber IOL (Alcon Labs, Forth Worth, TX, USA)
Hydrophilic Acrylic	Model Akreos Fit, 5.75 mm biconvex soft, foldable, posterior chamber IOL disk optic (Bausch & Lomb, Rochester, NY, USA)
Silicone	Model 911A CeeOn Edge, 6.00 mm biconvex soft, foldable, UV absorbing optic posterior chamber IOL (Pharmacia Groningen BV, 9728 NX Groningen, The Netherlands)

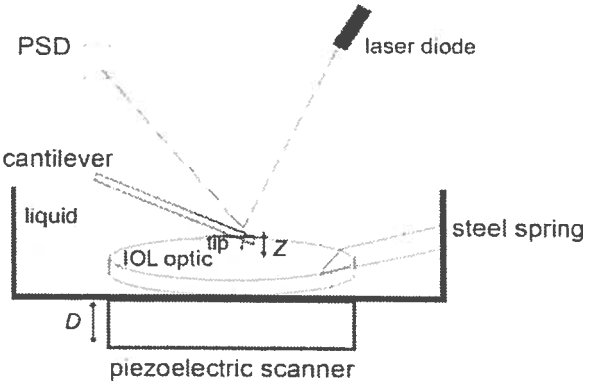

Figure 1. A schematic view of an intraocular lens (IOL) liquid cell for AFM measurements. The IOL consists of a central optic supported by haptics which provide support in the eye. The IOL sample was placed on a mold and glued with epoxy glue with the anterior surface optic side facing downwards. Maximum attention was paid during these maneuvers not to damage the IOL or alter the surface curvature. AFM topographic and nanomechanical measurements were made with the tip and the IOL surface completely immersed in liquid.
The position of the sample is adjusted by the piezoelectric translator. The deflection of the cantilever is usually measured using the *optical lever technique*. A beam from a laser diode is focused onto the end of the cantilever and the position of the reflected beam is monitored by a position sensitive detector (PSD). Exclusively for adhesion measurements, both the sample and tip were immersed in deionised water. This was done in order to avoid the meniscus force, that would otherwise dominate Van der Waals and any other weaker interactions, and to minimize the effect of *double-layer forces*, due to the charging of both sample and tip surfaces in liquid.
To highlight details, the figure has not been scaled.

The three-dimensional (3-D) topography measurements of the IOLs' optic were performed using an Autoprobe CP (Veeco, Sunnyvale, CA, USA), using V-shaped, silicon nitride cantilevers

(Veeco, CA, USA) with a tip curvature of 30 nm and nominal spring constant of 0.01 Newton/meter (N/m). The measurements were performed in contact mode with the tip and the sample completely immersed in balanced salt solution (BSS). All the reported images were acquired at a scan rate of 1 Hz per line and with a 256 x 256 pixel image definition. Image processing included only flattening (2^{nd} order) to remove the background slope due to the irregularities of the piezoelectric scanner. The analysis was performed using special image analysis software of the AFM (ProScan 1.5, Veeco, CA, USA). In this work the surface morphology was evaluated to obtain information on the root mean square of the roughness within a given area (*RMS roughness)*, that is the standard deviation of the height data. The roughness measurements were performed, for each sample, on ten reference areas of 10 x 10 μm of high-quality images on different locations of the IOL surface to verify the reproducibility of the observed features. The Kruskal-Wallis test was used to statistically compare the differences among IOL types in surface roughness values. When statistical significance was found, the difference between two groups of IOLs was further compared using the Mann-Whitney *U* test. Differences with a *P* value of 0.05 or less were considered statistically significant.

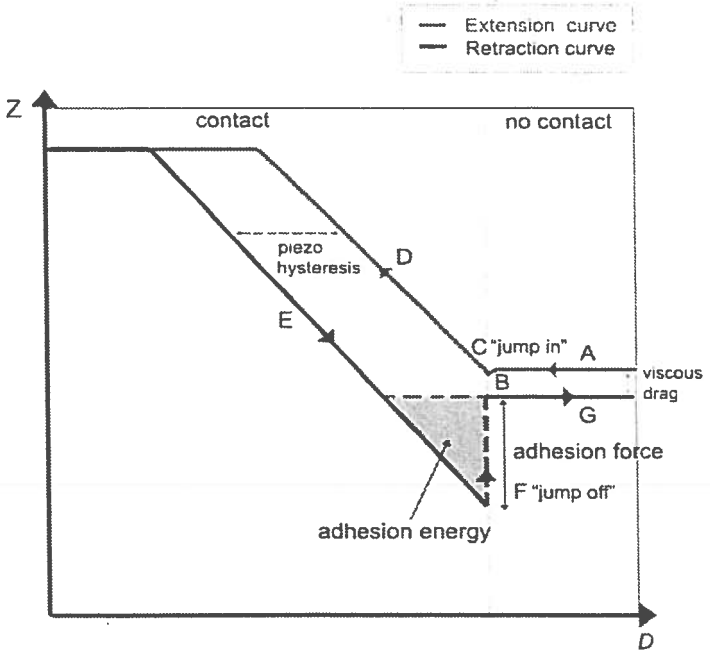

Figure 2. Different parts may be distinguished in the graphical representation of a *f-d* curve: A) at large separation, the interaction between the sample and probe is zero (no contact region); B) as the sample's surface approaches the probe, the cantilever may bend upwards due to the repulsive forces (double-layer forces); C) until the probe jumps into contact when the gradient of forces (attractive) exceeds the spring constant of the cantilever, k_c ("jump-in"). D) when the force is increased in the contact region, the shape of the approach curve may provide direct information on the material properties of the sample (e.g., stiffness). E) Upon retraction of the sample's surface from the probe, the approach and retraction curves may not overlap, due to the difference in the piezo displacement versus applied voltage (piezo hysteresis). F) Tip and sample separate when the gradient of the adhesion forces becomes smaller than k_c ("jump-off") and the tip returns to its resting position (G). Contact and non-contact parts of the *f-d* curve are easily distinguishable. In a *f-d* plot, *Z* and *D* are the cantilever deflection and the piezo displacement respectively.

The adhesive properties of the IOLs' optic were measured using the NanoScope III (Veeco, Sunnyvale, CA, USA) in the Force-vs-Distance (*f-d*) mode [27,28]. To avoid capillarity and double layer forces, adhesion measurements were performed, at room temperature (21°C), in deionised water (figure 1), using rectangular silicon cantilevers of nominal elastic constant of 10 N/m (Nanoandmore GmbH, Wetzlar, Germany) [29]. The nominal value of the tip's radius of curvature was 1 μm and the scanning speed during the acquisitions was in the range 10-400 nm/s. We verified that in this range the measurements were independent from the scanning rate. A probe with a micrometer sized tip has been chosen for two reasons: first, a large radius of curvature allows better precision in determining the adhesive forces; second, a large radius helps prevent damage to the sample.

In the *f-d* mode of AFM, forces applied on the sample's surface are measured by the deflection of the cantilever while approaching and retracting from the sample's surface. In our study, force measurement relies on the IOL sample being repeatedly approached towards and retracted away from the tip. Within the extension-retraction cycle, a signal proportional to the deflection of the cantilever (Z) is recorded as a function of the vertical position (D) of the piezoelectric stage. In order to transform the arbitrary deflection of the cantilever into a *f-d* curve, first the photo-sensitive detector (PSD) sensitivity should be known (it can be determined as the slope of the curve in the contact region, as shown in figure 2), then Z can be converted into units of force (nanoNewton, nN) according to the Hooke's law: $F = k_c \cdot Z$, where k_c is the cantilever elastic constant. The probe-sample separation d is then evaluated as the sum of the piezo displacement and the cantilever deflection, as following: $d = D + Z$. A Matlab routine (software version 7.0, The MathWorks, Inc.) was implemented to convert the AFM raw deflection data (D and Z) into a force profile.

Figure 2 is a schematic picture of a *f-d* curve during a full cycle. It consists of two parts: the approach and the withdrawal curve, acquired while the sample is moved vertically towards the tip and back. The gray curve corresponds to the force measured while approaching (run-in) the probe towards the sample, the black curve represents the force measured while retracting (run-out) it. Each curve can be further divided into a *no-contact region*, where the probe-sample interaction is negligible and the cantilever deflection is zero, a *contact region*, where the probe is indeed in contact with the sample surface and an *intermediate region* (dashed gray line) where the probe and the sample are at close distance and the cantilever is deflected by the van der Waals and electrostatic forces. Any difference between the approach and retraction is called "*f-d* curve hysteresis". The hysteresis of the curve in figure 2 shows three main features: the first is the vertical offset in the no-contact region. It is only present when working in liquid and is mainly due to hydrodynamic drag on the cantilever, which produces a force in the direction opposite to the movement of the cantilever [30]. The second feature is horizontal offset in the contact region. Responsible of the offset are the hysteresis in the piezoelectric extension of the scanner [31] as well as plastic and viscoelastic deformation of the sample surface [32]. The last feature is hysteresis in the intermediate region. The hysteresis in this region is mainly due to the adhesive forces which tend to keep the surfaces in contact. In the run out, the elastic force of cantilever has to work against adhesion in order to separate the probe from the surface (*jump off*).

The experimental conditions and parameters of the force measurement were chosen to eliminate the effect of hydrodynamic drag. Hysteresis in the piezoelectric extension of the scanner was still present but did not affect the interpretation of the data.

The adhesion between the probe and the IOL surface was measured from the minimum of the run-out: the difference between the minimum of this curve and the tip's resting position is proportional to the maximum adhesion force (F_{ad}). The adhesion energy (W_{ad}), that is equal to the gray area in figure 2, was further measured.

For statistical analysis, both the F_{ad} and W_{ad} were calculated on 50 curves taken in the central region of the posterior optic of each analyzed IOL. All data used for statistical analysis were acquired using the same cantilever. This procedure was used to avoid any bias that may have been introduced by both cantilever elastic constant calibration and different probe radius. The one-way analysis of variance (ANOVA) test was used to statistically compare the differences among IOL types in F_{ad} and W_{ad} values. When statistical significance has been found, the differences between IOLs were further compared using the Tukey test for pairwise comparisons. Differences with a P value of 0.05 or less were considered statistically significant.

RESULTS

Although all the IOL surfaces were relatively smooth, AFM investigation demonstrated statistically significant differences in the surface roughness values between IOL optics of various materials ($P<0.001$, Kruskal-Wallis test). Table 2 summarizes the quantitative IOLs' surface roughness analysis. The PMMA IOL optic had more surface irregularities than the other types of IOL biomaterials ($P<0.001$). No significant differences were observed in the *RMS roughness* values between the hydrophobic acrylic and silicone IOLs ($P>0.05$, Mann-Whitney U test). In addition, AFM measurements revealed that the surfaces of soft hydrophobic IOLs were smoother than the surfaces of the soft hydrophilic IOL ($P<0.05$).

The topographic images of the PMMA lens surfaces demonstrated numerous grooves with different orientations. These lines are to be related to the manufacturing processes of this type of lens. IOLs are prepared from PMMA polymer using a lathe-cutting tools. After cutting to the specified dimensions, the optic surface of the IOL is tumble polished. At the end of the fabrication process the posterior surface of the IOL is polished until the correct base curve is achieved [33]. Hence, scratch lines may be produced during the lathing and polishing processes. The topographic analysis of these linear features revealed a mean depth of 0.07 ± 0.01 nm and a mean width of 235 ± 45 nm. The typical appearance of PMMA lenses tested with numerous intersecting scratch lines is illustrated in figure 3.

Table 2. Measurement of the roughness parameters for the posterior surface of the IOLs performed on reference areas of 100 μm^2 of the lens optic surface. The total investigated are was 4000 μm^2 for each type of IOL

IOL material	RMS roughness (nm, M ± SD)*
PMMA	7.0 ± 0.6
Hydrophobic Acrylic	3.8 ± 0.2
Hydrophilic Acrylic	5.0 ± 0.5
Silicone	4.0 ± 0.5[*]

* Statistical significance among IOL materials: $P<0.001$

[*] Data for silicone IOL were measured with AFM in air and in no-contact mode

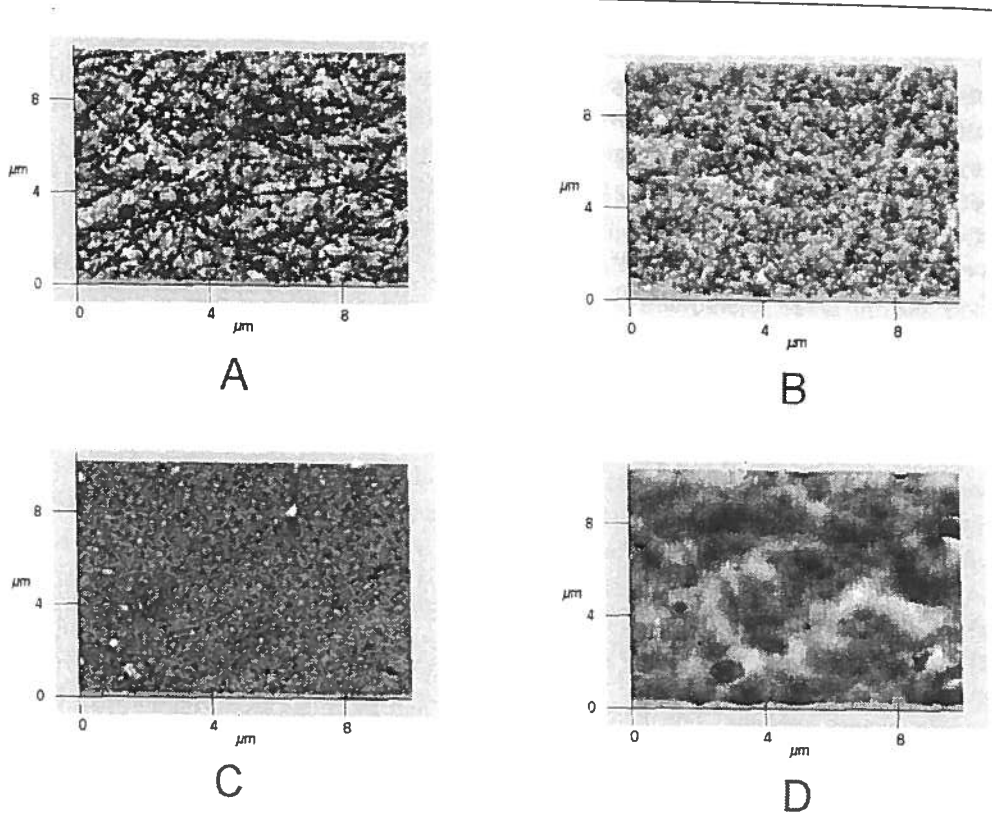

Figure 3. Atomic Force Microscopy imaging of the posterior surface of the PMMA (A), silicone (B), hydrophilic acrylic (C) and hydrophobic acrylic (D) IOLs. Image scale is 10 x 10 µm. The PMMA images revealed distinct grooves irregularly distributed all over the surface optic. These scratch lines may be produced during the fabrication processes of this type of IOL. The silicone IOL showed numerous protruding micro-granular features and infrequent ridge-like structures intersecting each-others. All the acrylic lenses revealed distinct pores at the posterior surface optic, varying in depth and dimensions between the various type of IOLs.

The surface of either the hydrophilic or hydrophobic acrylic IOLs showed pores of similar distribution but with varying densities and sizes among types (figure 3). The hydrophobic acrylic IOL showed pores of larger dimensions (mean depth of 1.2 ± 0.2 nm and mean diameter of 596 ± 157 nm) than that of the hydrophilic acrylic lens, which showed numerous diffuse small pits (mean depth of 0.8 ± 0.2 nm and mean diameter of 142 ± 25 nm).

The imaging of silicone IOL was extremely difficult to operate in contact AFM mode in liquid, because of unstable contact between the tip and the sample. Even if the very low elastic constant lever of 0.01 N/m was used, the tip damaged the sample surface. Silicone IOL was then imaged in air using no-contact AFM mode and with this method we did not experience any sample surface damage. Regular micro-granular features and infrequent ridge-like structures, with a mean high of 0.8 ± 0.1 nm and a mean width of 141 ± 24 nm, were observed all over the surface optic of this type of IOL biomaterial, as shown in figure 3.

As it regards the adhesion measurements, one should bear in mind that the adhesion force F_{ad} is a combination of the electrostatic force F_{el}, the van der Waals force F_{vdW}, the meniscus or capillary force F_{cap} and forces due to chemical bonds or acid–base interactions, F_{chem}, where: $F_{ad} = F_{el} + F_{vdW} + F_{cap} + F_{chem}$. In aqueous solutions, the F_{cap} is removed, as explained

in the legend to figure 1, and electrostatic forces become relatively more important since most surfaces are charged due to dissociation of surfaces groups. On the other hand, their magnitude depends on electrolyte concentration: therefore, using deionised water, one can greatly minimize their contribution, in addition to the contribution of F_{chem}. In this experiment, F_{vdW}, definitely, made the largest contribution to F_{ad}.

Figure 4 shows the typical curves acquired for each IOL material. The results on the surface adhesion properties of each IOL are summarized in table 3. Values were significantly different among IOLs of various materials (ANOVA, $P<0.001$). The mean F_{ad} value was highest on the hydrophobic acrylic IOL (283.75 ± 0.14 nanoNewton, nN), whereas the force curves acquired on silicone IOL (2.10 ± 0.01 nN) had the smallest attraction between the tip and the sample's surface. A direct comparison of each pair of IOLs found statistically significant differences (Tukey, $P<0.001$). The mean W_{ad} value measured was highest for the hydrophobic acrylic IOL, 9.70 ± 0.06 femtoJoule (fJ) and lowest for the silicone IOL (0.60 ± 0.01 fJ).

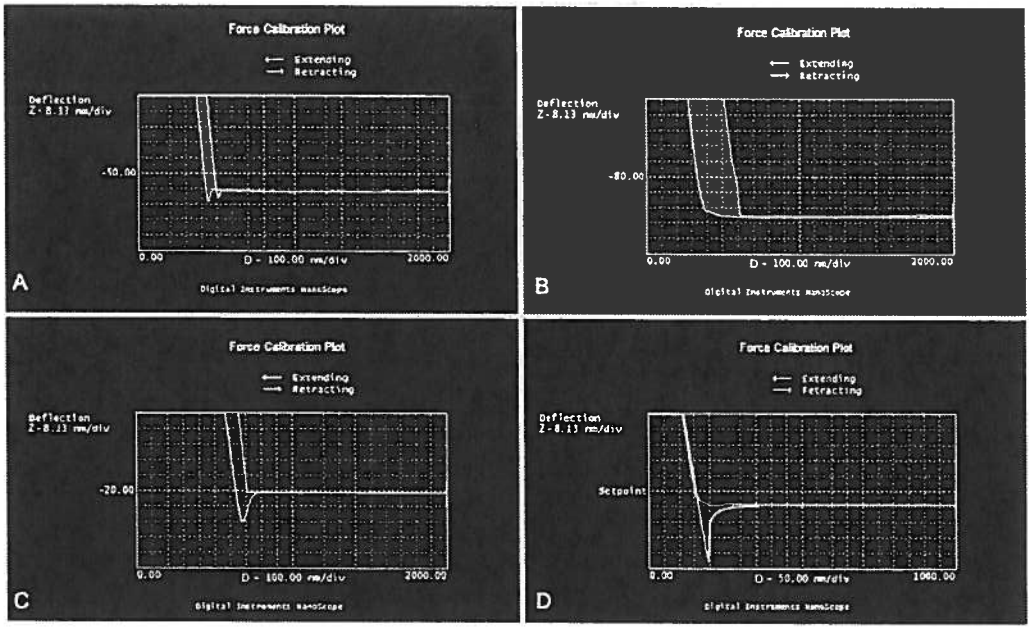

Figure 4. One typical extension-retraction cycle for each type of IOL material tested is shown. In A, B, C and D, the curves of PMMA, silicone, hydrophilic acrylic and hydrophobic acrylic IOLs respectively are shown. In the *x*- and *y*-axis are the sample displacement position (*D*, nm/div) and the cantilever deflection (*Z*, nm/div) respectively. Knowing the PSD sensitivity and k_c, the F_{ad} can be calculated according to the Hooke's law, as summarized in the text.
No plastic or viscoelastic deformation of the sample surface has occurred. This was confirmed by the reproducibility of the data as well as the fact that both trace and retrace show the same slope in the contact region.
The adhesiveness properties of the sample surface can be extracted from *f-d* curves examining the response of the material to unloading. Upon retraction, the maximum cantilever deflection was observed for the hydrophobic acrylic IOL, the minimum for the silicone IOL.

Table 3. Mean (± SD) adhesion force and adhesion energy measurements calculated in the central region of the posterior optic surface for each type of IOL

IOL material	Adhesion force (nanoNetwon, nN)*	Adhesion energy (femtoJoule, fJ)*
PMMA	45.77 ± 0.47	1.64 ± 0.01
Hydrophobic Acrylic	283.75 ± 0.14	9.70 ± 0.06
Hydrophilic Acrylic	84.76 ± 0.94	3.49 ± 0.04
Silicone	2.10 ± 0.01	0.60 ± 0.01

* Statistical significance among IOL materials: $P<0.001$

Multiple *f-d* curves were recorded on different areas of the central posterior optic surface and always showed the same features, indicating that the IOL surface was homogeneous as chemico-physical properties. Moreover, for each position, no modification in the adhesion was seen with repeated contacts. AFM imaging, performed immediately after each *f-d* measurement course, confirmed that the IOL surface morphology was not modified nor damaged during the course of the force measurements. This test was done to further verify that adhesion determination was not altered by irreversible changes in the sample.

DISCUSSION

There has been a long debate on theories and techniques to prevent PCO in clinical ophthalmology research. In general, the literature agrees that new surgical techniques and IOL optic designs contributed to a decrease in PCO rate in recent years [2,7]: a sharp posterior optic edge is currently considered to be the major factor in preventing PCO, regardless of the IOL material, because the edge provides a barrier to LECs migration [2,15,16,17,34,35,36,37]. This was verified with different IOL materials including PMMA, acrylate and silicone [26,38,39]: On the other hand, the exact influence of the IOL material on PCO prevention is not yet entirely understood, mainly due to the complexity of managing long-term, prospective clinical studies directly comparing the PCO rate after implantation of IOLs of various materials and optic designs [1,2,3,4,5,20,23,36,40,41].

As cells move toward a solid surface, the initial interaction between the cell and the biomaterial is governed by long and medium range forces, primarily van der Waals and electrostatic forces, that are strongly dependent on the chemico-physical properties of the respective surfaces. Atomic Force Microscopy can reliably analyze these surface interactions non-destructively in liquids, i.e., in condition similar to the ocular environment, and provide quantitative information on the surface properties of biomaterials with a nanometer-resolved spatial resolution, relevant to the size of cells-surface material interactions.

In this study, we investigated the surface roughness, topography and adhesiveness of various types of intraocular lenses exploiting the AFM technique. AFM is one of the numerous types of scanning probe microscopy techniques. Unlike traditional microscopes, scanning probe systems do not use lenses, so their resolution is limited by the size of the probe rather than diffraction effects [42].

The topography of the sample is obtained through an optical system by plotting the deflections of the small, flexible probe as a function of its position on the sample. The advantages of AFM are the acquisition of three-dimensional images of the surface topography of solid interfaces, direct quantitative height information from the images obtained and analysis of samples under near use conditions in ambient air or liquids. More information on the AFM techniques in ophthalmology were discussed in previous works [43,44].

In this work, we measured significant different surface features between the IOLs with respect to the lens biomaterial, probably dependent on the IOL fabrication processes [33,45]. It is likely that surface optic topography of IOLs produced by different manufacturers may vary depending on the different manufacturing processes used. AFM topographic measurements demonstrated statistically significant differences between the optic surface roughness of various IOL materials. PMMA IOL had the highest roughness, with more surface irregularities than the soft lens materials. Among these, the hydrophobic IOL revealed a smoother surface than the hydrophilic lens. In the literature, PMMA IOLs were associated with the greatest incidence of PCO [1,2,4,7,46]. A recent review confirmed how a polished optical surface of the IOL can play a major role in reducing cell adhesion and invasion of LECs over the IOL optic [47]. In addition, the amount of surface irregularities has been found to be linearly related to the number of inflammatory cells adhering to the optic surface of the IOL and to the rate of LEC migration [25,48]. Hence, the submicrometric morphology and regularity of the IOL optic surface should be a key factor for influencing both the adhesion and migration of LECs over the IOL optic [23,25].

After determining the surface topography and roughness of IOLs, we focused our research on the adhesive properties of the IOL materials. AFM can further provide valuable information on the nano-mechanical properties of solid interfaces, like stiffness and adhesion. Currently, the growth of direct force measurements via *force*-vs-*distance* curves obtained by AFM offered new ways to investigate the biomaterial-aqueous interface [27,28,29]. Indeed, the adhesiveness of the IOL material to the lens capsule has been theorized to be one of the most desirable IOL properties to minimize PCO. Since the capsular bend requires weeks to be completely formed [19,34], a quick and firm contact between the IOL material and the capsule likely represents itself the first factor to inhibit the migration of LECs in the space between the IOL and capsule, enhancing PCO prevention.

During the last years, researchers highlighted the role of the IOL surface adhesion characteristics in influencing the incidence and severity of PCO formation, regardless of the IOL design. Several clinical and experimental studies [24,49] determined qualitatively the adhesion of various IOL materials to the lens capsule, demonstrating a stronger adhesion for acrylic IOLs than PMMA or silicone IOLs. A varying degree of adhesion and migration of LECs onto the IOL surface depending on the IOL material was further demonstrated [36,50,51,52].

The study of AFM *f-d* curves provided a deeper knowledge of the bio-adhesive properties of IOL materials. A stronger adhesiveness has been measured at the surface optic of acrylic IOLs in comparison with PMMA and silicone IOLs, as argued by a previous work [24]. In theory, the tacky nature of the acrylic implant can lead to an increased adhesion to the lens capsule. By binding quickly and tightly to the capsular bag, a more adhesive IOL disc optic may limit the LEC migration onto the posterior capsule in the days after surgery, playing a key contributing role in PCO prevention [19,34]. In this context, several clinical studies have

yet demonstrated less PCO incidence following implantation of acrylic IOLs than other materials [1,20,22,23,49], regardless of the IOL optic design.

Statistically significant differences were further determined in our study between hydrophobic and hydrophilic acrylic materials. This result could be explained in terms of the hydrophobic effect. In aqueous environment, hydrophobic interactions usually give the highest adhesion force [53]. The measured difference in surface disk optic adhesiveness between acrylic materials may additionally play a role in preventing PCO, as clinically reported [54].

Besides the type of IOL biomaterial or the optic edge design, additional factors may contribute to influence the cellular behaviour at the capsule-lens interface: these include haptic angulation, design and stiffness, that can contribute to actively press the IOL against the capsule; the elasticity and deformation of the capsule itself [55,56]; and the adsorption of extracellular molecules, secreted by inflammatory cells or LECs, onto the IOL optic. Indeed, protein molecules were stated to play a not secondary role in the adhesion mechanism. Authors hypothesized.that if an IOL has more fibronectin bound to it, the IOL can also attach to the capsule better as it consists mainly of collagen [57]. Fibronectin was further measured to adhere more onto hydrophobic acrylic IOLs than on PMMA, silicone or hydrophilic acrylic lenses [57,58].

Another consideration is that IOLs of the same material from different manufactures can have different surface properties. Using three different hydrophobic acrylic IOLs, researchers [59] have demonstrated how the adhesiveness of disk optics of the same material and design from a single manufacture can change dramatically because of differences in the surface energy caused by modification of the copolymers' constituents. It is, in fact, well known that modifying the surface energy of the IOL optic can influence the adhesiveness of the material [59,60,61].

In conclusion, the results of this study demonstrated the efficacy and accuracy of the AFM as a research tool for the analysis of biomaterials that are used in the ophthalmology surgical practice. These types of measurements on IOLs can be useful for improving the manufacturing processes and testing experimental approaches to improve biocompatibility and minimize the risk of PCO [47].

Further studies are necessary to elucidate the mechanism of PCO development and the interface interactions between the IOL and capsule.

REFERENCES

[1] Findl, O; Menapace, R; Sacu, S; Buehl, W; Rainer, G. Effect of optic material on posterior capsule opacification in intraocular lenses with sharp-edge optics. Randomized clinical trial. *Ophthalmology*, 2005, 112, 67-72.

[2] Kohnen, T; Fabian, E; Gerl, R; Hunold, W; Hütz, W; Strobel, J; Hoyer, H; Mester, U. Optic edge design as long-term factor for posterior capsular opacification rates. *Ophthalmology*, 2008, 115, 1308-1314.

[3] Mester, U; Fabian, E; Gerl, R; Hunold, W; Hütz, W; Strobel, J; Hoyer, H; Kohnen, T. Posterior capsule opacification after implantation of CeeOn Edge 911A, PhacoFlex SI-

40NB, and AcrySof MA60BM lenses: one-year results of an intraindividual comparison multicenter study. *J Cataract Refract Surg.*, 2004, 30, 978-985.

[4] Apple, DJ; Peng, Q; Visessook, N; Werner, L; Pandey, SK; Escobar-Gomez, M; Ram, J; Auffarth, GU. Eradication of posterior capsule opacification: documentation of a marked decrease in Nd:YAG laser posterior capsulotomy rates noted in an analysis of 5416 pseudophakic human eyes obtained postmortem. *Ophthalmology*, 2001, 108, 505-518.

[5] Sacu, S; Menapace, R; Wirtitsch, M; Buehl, W; Rainer, G; Findl, O. Effect of anterior polishing on fibrotic capsule opacification: three-year results. *J Cataract Refract Surg.*, 2004, 30, 2322-2327.

[6] Hollick, EJ; Spalton, DJ; Meacock, WR. The effect of capsulorhexis size on posterior capsular opacification: one-year results of a randomized prospective trial. *Am J Ophthalmol*, 1999, 128, 271-279.

[7] Findl, O; Buehl, W; Bauer, P; Sycha, T. Interventions for preventing posterior capsule opacification. *Cochrane Database Syst Rev.*, 2007, 18, CD003738.

[8] Lois, N; Dawson, R; McKinnon, A; Forrester, JV. A new model of posterior capsule opacification in rodents. *Invest Ophthalmol Vis Sci.*, 2003, 44, 3450-3457.

[9] Majima, K; Majima, Y. Shape of lens epithelial cells after intraocular lens implantation. *J Cataract Refract Surg.*, 2001, 27, 745-752.

[10] Abela-Formanek, C; Amon, M; Schild, G; Schauersberger, J; Heinze, G; Kruger, A. Uveal and capsular biocompatibility of hydrophilic acrylic, hydrophobic acrylic, and silicone intraocular lenses. *J Cataract Refract Surg.*, 2002, 28, 50-61.

[11] Ohnishi, Y; Yoshitomi, T; Sakamoto, T; Fujisawa, K; Ishibashi, T. Evaluation of cellular adhesions on silicone and poly(methylmethacrylate) intraocular lenses in monkey eyes. An electron microscopic study. *J Cataract Refract Surg.*, 2001, 27, 2036-2040.

[12] Müllner-Eidenböck, A; Amon, M; Schauersberger, J; Kruger, A; Abela, C; Petternel, V; Zidek, T. Cellular reaction on the anterior surface of 4 types of intraocular lenses. *J Cataract Refract Surg.*, 2001, 27, 734-740.

[13] Tognetto, D; Toto, L; Ballone, E; Ravalico, G. Biocompatibility of hydrophilic intraocular lenses. *J Cataract Refract Surg.*, 2002, 28, 644-651.

[14] Shah, SM; Spalton, DJ. Comparison of the postoperative inflammatory response in the normal eye with heparin-surface-modified and poly(methylmethacrylate) intraocular lenses. *J Cataract Refract Surg.*, 1995, 21, 579-585.

[15] Buehl, W; Findl, O; Menapace, R; Rainer, G; Sacu, S; Kiss, B; Petternel, V; Georgopoulos, M. Effect of an acrylic intraocular lens with a sharp posterior optic edge on posterior capsule opacification. *J Cataract Refract Surg.*, 2002, 28, 1105-1111.

[16] Nagamoto, T; Fujiwara, T. Inhibition of lens epithelial cell migration at the intraocular lens optic edge. Role of capsule bending and contact pressure. *J Cataract Refract Surg.*, 2003, 29, 1605-1612.

[17] Nishi, O; Nishi, K; Wickström, K. Preventing lens epithelial cell migration using intraocular lenses with sharp rectangular edges. *J Cataract Refract Surg.*, 2000, 26, 1543-1549.

[18] Nishi, O; Nishi, K; Sakanishi, K. Inhibition of migrating lens epithelial cells at the capsular bend created by the rectangular optic edge of a posterior chamber intraocular lens. *Ophthalmic Surg Lasers*, 1998, 29, 587-594.

[19] Nishi, O; Nishi, K. Effect of optic size of a single-piece acrylic intraocular lens on posterior capsule opacification. *J Cataract Refract Surg.*, 2003, 29, 348-353.

[20] Li, N; Chen, X; Zhang, J; Zhou, Y; Yao, X; Du, L; Wei, M; Liu, Y. Effect of AcrySof versus Silicone or Polymethyl-methacrylate intraocular lens on posterior capsule opacification. *Ophthalmology*, 2007, 115, 830-838.

[21] Kurosaka, D; Kato, K. Membranous proliferation of lens epithelial cells on acrylic, silicone, and poly(methyl methacrylate) lenses. *J Cataract Refract Surg.*, 2001, 27, 1591-1595.

[22] Weyde, G; Kukelberg, M; ZetterstrÖm, C. Posterior capsule opacification: comparison of 3 intraocular lenses of different materials and design. *J Cataract Refract Surg.*, 2003, 29, 1556-1559.

[23] Hollick, EJ; Spalton, DJ; Ursell, PG; Pande, MV; Barman, SA; Boyce, JF; Tilling, K. The effect of polymethylmethacrylate, silicone, and polyacrylic intraocular lenses on posterior capsular opacification 3 years after cataract surgery. *Ophthalmology*, 1999, 106, 49-54.

[24] Oshika, T; Nagata, T; Ishii, Y. Adhesion of lens capsule to intraocular lenses of polymethylmethacrylate, silicone, and acrylic foldable materials: an experimental study. *Br J Ophthalmol*, 1998, 82, 549-553.

[25] Yamanaka, N; Tanaka, T; Shigeta, M; Hamano, M; Usui, M. Surface roughness of intraocular lenses and inflammatory cell adhesion to lens surfaces. *J Cataract Refract Surg*, 2003, 29, 367-370.

[26] Nishi, O; Nishi, K; Osakabe, Y. Effect of intraocular lenses on preventing posterior capsule opacification: design versus material. *J Cataract Refract Surg.*, 2004, 30, 2170-2176.

[27] Cappella, B; Baschieri, P; Frediani, C; Miccoli, P; Ascoli, C. Force-distance curves by AFM. A powerful technique for studying surface interactions. *IEEE Eng Med Biol.*, 1997, 16, 58-65.

[28] Butt, HJ; Cappella, B; Kappl, M. Force measurements with the atomic force microscope: technique, interpretation and applications. *Surf Sci Rep.*, 2005, 59, 1-152.

[29] Hodges, CS. Measuring forces with the AFM: polymeric surfaces in liquids. *Advances in Colloid and Interface Science*, 2002, 99, 13-75.

[30] Vinogradova, OI; Butt, HJ; Yakubov, GE; Feuillebois, F. Dynamic effects on force measurements. I. Viscous drag on the atomic force microscopy cantilever. *Rev Sci Instrum*, 2001, 72, 2330-2339.

[31] Hues, SM; Draper, CF; Lee, KP; Colton, RJ. Effect of PZT and PMN actuator hysteresis and creep on nanoindentation measurements using force microscopy. *Rev Sci Instrum*, 1994, 65, 1561-1565.

[32] Cappella, B; Stark, W. Adhesion of amorphous polymers as a function of temperature probed with AFM force-distance curves. *J Colloid Interface Sci.*, 2006, 2, 507-514.

[33] Sankar, V; Kumar, S; Rao, KP. Preparation, characterisation and fabrication of intraocular lens from photo initiated polymerised poly(methylmethacrylate). *Trends Biomater Artif Organs*, 2004, 17, 24-30.

[34] Nishi, O; Nishi, K; Akura, J. Speed of capsular bend formation at the optic edge of acrylic, silicone, and poly-(methylmethacrylate) lenses. *J Cataract Refract Surg.*, 2002, 28, 431-437.

[35] Kruger, AJ; Schauersberger, J; Abela, C; Schild, G; Amon, M. Two year results: sharp versus rounded optic edges on silicone lenses. *J Cataract Refract Surg.*, 2000, 26, 566-570.

[36] Schauersberger, J; Amon, M; Kruger, A; Abela, C; Schild, G; Kolodjaschna, J. Lens epithelial cell outgrowth on 3 types of intraocular lenses. *J Cataract Refract Surg.*, 2001, 27, 850-854.

[37] Nishi, O; Yamamoto, N; Nishi, K; Nishi, Y. Contact inhibition of migrating lens epithelial cells at the capsular bend created by a sharp-edged intraocular lens after cataract surgery. *J Cataract Refract Surg.*, 2007, 33, 1065-1070.

[38] Buehl, W; Findl, O. Effect of intraocular lens design on posterior capsule opacification. *J Cataract Refract Surg.*, 2008, 34, 1976-1985.

[39] Kruger, AJ; Schauersberger, J; Abela, C; Schild, G; Amon, M. Two year results: sharp versus rounded optic edges on silicone lenses. *J Cataract Refract Surgi.*, 2000, 26, 566-570.

[40] Findl, O; Menapace, R; Sacu, S; Buehl, W; Rainer, G. Effect of optic material on posterior capsule opacification in intraocular lenses with sharp-edge optics. *Ophthalmology*, 2005, 112, 67-72.

[41] Linnola, RJ. Sandwich theory: bioactivity-based explanation for posterior capsule opacification. *J Cataract Refract Surg.*, 1997, 23, 1539-1542.

[42] Sanchez-Sevilla, A; Thimonier, J; Marilley, M; Rocca-Serra, J; Barbet, J. Accuracy of AFM measurements of the contour length of DNA fragments adsorbed on mica in air and in aqueous buffer. *Ultramicroscopy*, 2002, 92, 151-158.

[43] Lombardo, M; De Santo, MP; Lombardo, G; Barberi, R; Serrao, S. Roughness of excimer laser ablated corneas with and without smoothing measured with atomic force microscopy. *J Refract Surg.*, 2005, 21, 469-475.

[44] Lombardo, M; De Santo, MP; Lombardo, G; Barberi, R; Serrao, S. Atomic Force Microscopy analysis of normal and photoablated porcine corneas. *J Biomechanics*, 2006, 39, 2719-2724.

[45] Lloyd, AW; Faragher, RG; Denyer, SP. Ocular biomaterials and implants. *Biomaterials*, 2001, 22, 769-785.

[46] Hayashi, K; Hayashi, H; Nakao, F; Hayashi, F. Changes in posterior capsule opacification after poly-(methyl methacrylate), silicone and acrylic intraocular lens implantation. *J Cataract Refract Surg.*, 2001, 27, 817-824.

[47] Saika, S. Relationship between posterior capsule opacification and intraocular lens biocompatibility. *Prog Ret Eye Res.*, 2004, 23, 283-305.

[48] Tanaka, T; Shigeta, M; Yamanaka, N; Usui, M. Cell adhesion to acrylic intraocular lens associated with lens surface properties. *J Cataract Refract Surg.*, 2005, 31, 1648-1651.

[49] Hollick, EJ; Spalton, DJ; Ursell, PG; Pande, MV. Lens epithelial cell regression on the posterior capsule with different intraocular lens materials. *Br J Ophthalmol*, 1998, 82, 1182-1188.

[50] Hesse, Y; Kampmeier, J; Lang, GK; Baldysiak-Figiel, A; Lang, GE. Adherence and viability of porcine lens epithelial cells on three different IOL materials in vitro. *Graefes's Arch Clin Exp Ophthalmol*, 2003, 241, 823-826.

[51] Kurosaka, D; Obasawa, m; Kurosaka, H; Nakamura, K. Inhibition of lens epithelial cell migration by an acrylic intraocular lens in vitro. *Ophthalmic Res.*, 2002, 34, 29-37.

[52] Versura, P; Torreggiani, A; Cellini, M; Caramazza, R. Adhesion mechanisms of human lens epithelial cells on 4 intraocular lens materials. *J Cataract Refract Surg.*, 1999, 25, 527-533.

[53] Israelachvili, JN. In: Intermolecular and surface forces, with applications to colloidal and biological systems, 2nd ed. San Diego, CA, *Academic Press*, 1992, 128-131.

[54] Scaramuzza, A; Fernando, GT; Crayford, BB. Posterior capsular opacification and lens epithelial cell layer formation: hydroview hydrogel versus acrysof acrylic intraocular lenses. *J Cataract Refract Surg.*, 2001, 27, 1047-1054.

[55] Boyce, JF; Bhermi, GS; Spalton, DJ; El-Ostra, AR. Mathematical modelling of the forces between and intraocular lens and the capsule. *J Cataract Refract Surg.*, 2002, 28, 1853-1859.

[56] Pedrigi, RM; David, G; Dziezyc, J. Regional mechanical properties and stress analysis of the human anterior lens capsule. *Vision Resi.*, 2007, 47, 1781-1789.

[57] Linnola, RJ; Sund, M; YlÖnen, R; Cand, M; Pihlajaniemi, T. Adhesion of soluble fibronectin, laminin, and collagen type IV to intraocular lens materials. *J Cataract Refract Surg.*, 1999, 25, 1486-1491.

[58] Linnola, RJ; Werner, L; Pandey, SK; Escobar-Gomez, M; Znoiko, SL; Apple, DJ. Adhesion of fibronectin, vitronectin, laminin, and collagen type IV to intraocular lens materials in pseudophakic human autopsy eyes. Part 1: histological sections. *J Cataract Refract Surg.*, 2000, 26, 1792-1806.

[59] Katayama, Y; Kobayakawa, S; Yanagawa, H; Tochikubo, T. The relationship between the adhesion characteristics of acrylic intraocular lens materials and posterior capsule opacification. *Ophthalmic Res.*, 2007, 39, 276-281.

[60] Burnham, NA; Dominguez, DD; Mowery, RL; Colton, RJ. Probing the surface forces of monolayer films with Atomic-Force Microscopy. *Phys Rev Lett*, 1990, 64, 1931-1934.

[61] Yuen, C; Williams, R; Batterbury, M; Grierson, I. Modification of the surface properties of a lens material to influence posterior capsular opacification. *Clin Experiment Ophthalmol*, 2006, 34, 568-574.